IEEE Access
Multidisciplinary | Rapid Review | Open Access Journal

Received January 29, 2017, accepted February 27, 2017, date of publication March 8, 2017, date of current version April 24, 2017.

Digital Object Identifier 10.1109/ACCESS.2017.2679223

Impact of Electrical Contact Resistance on the High-Speed Transmission and On-Line Diagnosis of Electrical Connector Intermittent Faults

QINMU SHEN, KEHONG LV, GUANJUN LIU, AND JING QIU

Science and Technology on Integrated Logistics Support Laboratory, College of Mechatronic Engineering and Automation, National University of Defense Technology, Changsha 410073, China

Corresponding author: J. Qiu (qiujing16@sina.com)

This work was supported by the National Natural Science Foundation of China under Grant 61403408.

ABSTRACT Electrical connectors are widely used in many kinds of main equipment. It is very difficult, costly, and time consuming for the off-line diagnosis of intermittent faults (IFs) in connectors. To realize the on-line diagnosis by the traditional method, the voltage drop between two ends of the connector should be measured continuously at a high sample rate. This continuous measurement requires enormous testing resources, which is impractical in engineering fields. To solve this problem, this paper proposes an on-line diagnosis method in condition of the single-end test for the electrical connector IFs. To determine the fault threshold of the electrical contact resistance (ECR), first the impact of the ECR on high-speed transmission is studied, and then the connector fault feature in condition of the single-end test, which is called the insertion loss increment (ILI), is extracted. The measurement method of the ILI is also presented. Based on the above analysis, an ILI-based on-line diagnosis method for the connector IFs is specified. According to the qualitative and quantitative tests, the proposed diagnosis method is verified. The verification results show that the cumulative insertion loss increment, which is calculated from the ILI can truly exhibit the variation of ECR, and the error of the ILI-based diagnosis method is only about 1%.

INDEX TERMS Electrical connector, electrical contact resistance, high-speed signal, intermittent fault, on-line diagnosis.

I. INTRODUCTION

The occurrence of intermittent fault (IF) is prevalent in various products, which will result in high maintenance costs and safety risks. IFs can cause no fault found (NFF), erroneous removal (ER), retest OK (RTOK) and other maintenance problems [1]. In 2012, a survey among 80 aerospace organizations showed that the IF was the main cause of NFF [2]. The NFF problem has become the highest cost source in the maintenance of aerospace equipment [3], [4].

As the fundamental electromechanical element, the electrical connectors are widely used to transmit electrical signals in different devices, systems and main complicated equipment. The fault of electrical connector is a widespread problem. Almost 70 percent of system failures are owing to the faults of elements, forty percent of which are owing to the faults of electrical connectors [5]. A field survey of warship faults performed by the authors shows that the interconnect faults account for more than 30% of all faults. Connector faults can result in serious problems, especially with their applications in aerospace, ship, submarine, high-speed rail and other complex fields.

The electrical connector IF is also called as the intermittence [6]–[8], which is fairly common [9]. The electrical connector IF is one of the main sources of NFF problem [10]. The fretting that can be induced by vibration is one of the main causes of electrical connector degradation. Since the important influence of fretting was elaborated by Bock and Whitley [11], many researchers have studied the effect of fretting on electrical contact, such as Antler [12], [13], Aukland *et al.* [14], Swingler and McBride [15], Malucci [16], etc.. In particular, Bryant [17] developed the fretting failure model for the electrical connector. Flowers *et al.* [18], [19] studied the effect of vibrational acceleration and frequency on ECR during fretting. Previous studies mainly focus on the mechanisms [7], [8], [20]–[22] and the occurrence laws [6], [8], [23] in terms of intermittence. Some researchers have

also studied the impact of contact performance on high-speed signal transmission [24]–[26].

However, there are only a few approaches for intermittence detection. They mainly fall into three types. First, find the signal accident by the signal process method and make decision by the cluster analysis method. This approach is developed only for particular components [27], [28]. Second, measure the signal in single end, and then find the abnormity of parameters for the transmission model. It is developed for the power delivery interconnections, as in this case the supply signals are determinate [29], [30]. Third, the particular instrument or device is used to detect the IF, such as the astronics arcsafe wire integrity tester (AAWIT) [31], the intermittent fault detection and isolation system (IFDIS) [3], the time domain reflectrometry (TDR) and the frequency domain reflectrometry (FDR) [2]. In particular, the IFDIS, which has been used in application, can simultaneously detect the defects and intermittences of hundreds of interconnection paths. However, this system can only be applied for the off-line diagnosis. Although the detection is fast, it may take a long time to fix the probes. Furthermore, the tested devices are singled out. This may make the fault detection not cover all the faulty units.

The connector fault, especially the IF, will propagate in both the longitudinal and transverse directions in a system and be confused with the faults of the connected parts, which will result in intricate fault symptoms, and then make it very hard to isolate the fault. In particular, the intermittent characteristic of the fault will make it require extensive manpower and time to test repeatedly and replace suspicious parts, and then run the device tentatively. If the traditional test approach is adopted for on-line diagnosis, the voltage drop between two ends of the connector should be measured continuously [7], [23], [32], [33]. This continuous measurement requires an additional test channel. Considering the numerous quantities of used connectors, this approach is impractical in practice. However, if the IF could be detected in the case that only one end of the connector is tested, the additional test channel would be unnecessary. Thus it would be possible to realize on-line diagnosis.

This study aims to on line diagnose the connector IFs in condition of the single-end test. To determine the fault threshold of the electrical contact resistance (ECR), the transmission characteristics of the electrical connectors in the transmit path are first analyzed in Section II. Accordingly, the impact of the ECR on the high-speed signal transmission is identified. In Section III, the fault features of the connectors in condition of the single-end test are analyzed. These features are referred to as insertion loss increments (ILIs). The method of measuring the ILIs is also presented. According to the results of the analysis, the ILI-based on-line diagnosis method for a connector IF is proposed in Section IV. Finally in Section V, the efficiency of the proposed diagnosis method is verified by way of the qualitative and quantitative approaches.

II. IMPACT OF ECR ON HIGH-SPEED SIGNAL TRANSMISSION

A. REVIEW OF TRANSMISSION LINE

The signal propagates in the conductor at a velocity v. When the signal passes through the interconnection with length l, the time delay is

$$t_d = \frac{l}{v} = \frac{l\sqrt{\varepsilon_r \mu_r}}{c}, \tag{1}$$

where ε_r is the relative dielectric constant. The variable μ_r is the relative magnetic conductivity of the material, which is one for most materials.

During the rise time t_r the signal propagation length in the interconnection is called the spatial extent of the leading edge, which is computed as

$$L_r = t_r \times v. \tag{2}$$

When the next formula is satisfied, the transmission line effect of the interconnection cannot be neglected. In this case, the transmitted signal should be seen as a high-speed signal, and then the signal integrity (SI) problems of the transmitting path should be considered.

$$\frac{t_r}{t_d} \leq \theta_h \quad L_r/l \leq \theta_h, \tag{3}$$

where θ_h is the threshold. In [34], [35], the threshold is set as 10.

For example, when a digital signal with a frequency of 1 MHz and rise time of 70 ns transmits in a RG58 coaxial cable, whose relative dielectric constant is 1.6453, the spatial extent of the leading edge L_r will be 16.37 m. When the interconnection is longer than $L_r/10 = 1.637$ m, the transmitted signal should be considered as a high-speed signal. It can be seen that the length is not great. For the connectors between devices, the cables are generally long enough at both sides, so the transmission line effect cannot be neglected even when the frequency of the transmitted signal is not high. In brief, when equation (3) is satisfied, the cable should be taken as a transmission line.

In terms of a uniform transmission line, the instantaneous impedance is constant and will be referred to as the characteristic impedance of the transmission line. When the impedance is not consecutive in the transmit path, the signal will be reflected. The reflection coefficient is defined as the ratio of the reflected voltage to the incident voltage, which is computed as

$$\Gamma_b = \frac{Z_2 - Z_1}{Z_2 + Z_1}, \tag{4}$$

where Z_1 is the characteristic impedance of the initial segment and Z_2 is the characteristic impedance of the new segment.

The transmission coefficient is defined as the ratio of the transmission voltage to the incident voltage and is computed as

$$\Gamma_f = \frac{2Z_2}{Z_2 + Z_1}. \tag{5}$$

When there are multi-discontinuities in a transmission path, the signal will be reflected over and over. Multiple signals will be superimposed and result in a complex waveform, and therefore the discontinuity of impedances should be eliminated in the design process. However, when the IF happens in the connector, the reflection will be inevitable, which will induce signal distortion and errors. Therefore, it is particularly necessary to analyze the impact of the ECR on the signal transmission.

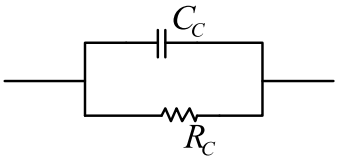

FIGURE 1. Equivalent circuit for electrical contact.

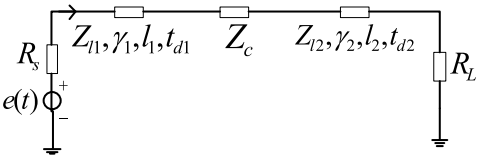

FIGURE 2. Equivalent circuit for the whole transmission path.

B. CONNECTOR EQUIVALENT CIRCUIT OF THE TRANSMISSION PATH

In recent years the equivalent circuit of electrical contact has been developed [25], [26], as shown in Fig. 1. This circuit includes two elements, i.e., the ECR and the electrical contact capacitance (ECC). The contact impedance can be computed as

$$Z_C = \frac{R_C}{1 + j\omega R_C C_C}, \tag{6}$$

where ω denotes the angular frequency of the signal, R_C denotes the ECR, and C_C denotes the ECC.

When the connector is fixed into the cables, the equivalent circuit of the whole transmission path is shown in Fig. 2. The ith transmission line is with the characteristic impedance Z_{li}, propagation constant γ_i, length l_i, and time delay t_{di}. Generally, it is assumed that $Z_{l1} = Z_{l2} = Z_0$.

C. PERFORMANCE IN THE FREQUENCY AND TIME DOMAIN

In view of the equivalent circuit shown in Fig. 2, the first transmission line, the connector, and the second transmission line form the two-port network. The signals are formalized in the complex frequency domain. The circuit model is transformed into a two-port network model, as shown in Fig. 3.

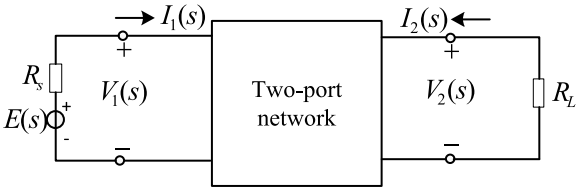

FIGURE 3. Two-port network model for the whole transmission path.

According to the impedance matrix, the port voltage and port current are formularized as

$$V = \begin{bmatrix} V_1 \\ V_2 \end{bmatrix} = \begin{bmatrix} Z_{11} & Z_{12} \\ Z_{21} & Z_{22} \end{bmatrix} \begin{bmatrix} I_1 \\ I_2 \end{bmatrix} = Z_T I. \tag{7}$$

They also satisfy the formulas

$$\begin{cases} V_1(s) = E(s) - R_s I_1(s) \\ V_2(s) = -R_L I_2(s). \end{cases} \tag{8}$$

Combining (7) and (8), we obtain

$$\begin{cases} E(s) - R_s I_1(s) = Z_{11} I_1(s) + Z_{12} I_2(s) \\ -R_L I_2(s) = Z_{21} I_1(s) + Z_{22} I_2(s). \end{cases} \tag{9}$$

The equations in (9) are solved to obtain the transfer function between the output voltage $v_2(t)$ and the input voltage $e(t)$, which is formularized as

$$H_{2/0}(s) = \frac{V_2(s)}{E(s)} = \frac{R_L Z_{21}}{-Z_{21}Z_{12} + (R_s + Z_{11})(R_L + Z_{22})}. \tag{10}$$

Until now, the elements in the impedance matrix are still unknown. The ABCD matrix will be used to compute these elements. The ABCD matrix of the ith transmission line is

$$A_i = \begin{bmatrix} \cosh(\gamma_i l_i) & Z_0 \sinh(\gamma_i l_{1i}) \\ \sin(\gamma_i l_i)/Z_0 & \cosh(\gamma_i l_i) \end{bmatrix}, \tag{11}$$

where $\sinh x = (e^x - e^{-x})/2$, $\cosh x = (e^x + e^{-x})/2$.

The ABCD matrix of the connector can be formularized as

$$B = \begin{bmatrix} 1 & Z_c \\ 0 & 1 \end{bmatrix}. \tag{12}$$

Calculating in a cascade form, the ABCD matrix of the two-portnetwork in Fig. 3 will be (13), as shown at the bottom of this page.

$$\begin{aligned} \mathrm{A}_T &= \begin{bmatrix} \mathrm{A}_{11} & \mathrm{A}_{12} \\ \mathrm{A}_{21} & \mathrm{A}_{22} \end{bmatrix} = A_1 B A_2 \\ &= \begin{bmatrix} \dfrac{Z_C \cosh(\gamma_1 l_1) \sinh(\gamma_2 l_2)}{Z_0} + \cosh(\gamma_1 l_1 + \gamma_2 l_2) & Z_C \cosh(\gamma_1 l_1) \cosh(\gamma_2 l_2) + Z_0 \sinh(\gamma_1 l_1 + \gamma_2 l_2) \\ \dfrac{Z_C \sinh(\gamma_1 l_1) \sinh(\gamma_2 l_2)}{Z_0^2} + \dfrac{\sinh(\gamma_1 l_1 + \gamma_2 l_2)}{Z_0} & \dfrac{Z_C \sinh(\gamma_1 l_1) \cosh(\gamma_2 l_2)}{Z_0} + \cosh(\gamma_1 l_1 + \gamma_2 l_2) \end{bmatrix} \end{aligned} \tag{13}$$

Thus, the impedance matrix can be calculated according to the ABCD matrix [36]

$$Z_T = \frac{1}{A_{21}} \begin{bmatrix} A_{11} & A_{11} \cdot A_{22} - A_{12} \cdot A_{21} \\ 1 & A_{22} \end{bmatrix}. \quad (14)$$

Substituting the elements of the impedance matrix in (14) into (10) and letting $\Gamma_s = R_s/Z_0$, $\Gamma_L = R_L/Z_0$, the transfer function in (10) can be simplified as

$$H_{2/0}(s) = \frac{\Gamma_L Z_0}{\eta_1 Z_C + \eta_2 Z_0}, \quad (15)$$

where

$$\begin{cases} \eta_1 = (\Gamma_s \sinh(\gamma_1 l_1) + \cosh(\gamma_1 l_1)) \\ \qquad \cdot (\Gamma_L \sinh(\gamma_2 l_2) + \cosh(\gamma_2 l_2)) \\ \eta_2 = (1+\Gamma_s\Gamma_L) \sinh(\gamma_1 l_1 + \gamma_2 l_2) \\ \qquad + (\Gamma_s + \Gamma_L) \cosh(\gamma_1 l_1 + \gamma_2 l_2). \end{cases}$$

According to the signal response on the linear time-invariant (LTI) system, the output waveform in the time domain $v_2(t)$ can be solved by

$$v_2(t) = \mathscr{F}^{-1}\{E(j\omega)H_{2/0}(j\omega)\}, \quad (16)$$

where $\mathscr{F}^{-1}(\cdot)$ represents the inverse Fourier transform. $E(j\omega)$ and $H_{2/0}(j\omega)$ are the Fourier transforms of the input signal and the transfer function, respectively.

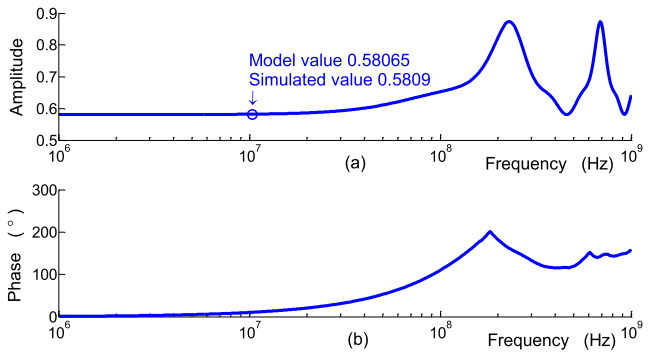

FIGURE 4. (a) and (b) Aplitude-frequency and phase-frequency characteristics, respectively, of the ILI.

For example, the involved parameters are set as follows: $R_C = 50\ \Omega$, $Z_0 = 75\ \Omega$, $C_C = 200$ fF, $R_s = 15\ \Omega$, $R_L = 90\ \Omega$, $t_{d1} = 1.086$ ns, and $t_{d2} = 2.172$ ns. The input signal is a square signal with a frequency of 10 MHz, rise time of 3 ns, and duty ratio of 50%. The model results will be compared to the HyperLynx simulation results. The amplitude-frequency and the phase-frequency characteristics obtained from (15) are shown in Fig. 4. The model and simulated values of attenuation at the frequency of 10 MHz are marked in Fig. 4(a). It indicates that the error is small. In the time domain the output waveform solved by (16) and the simulation waveform are consistent, as shown in Fig. 5.

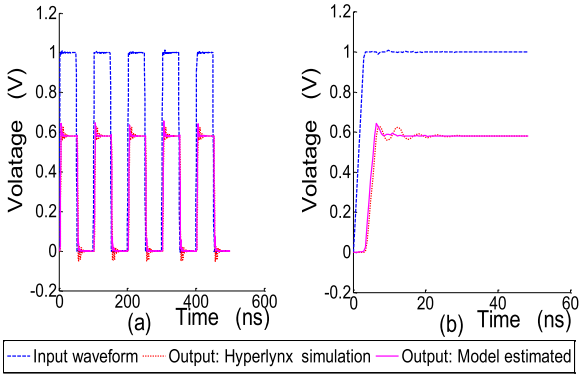

FIGURE 5. Comparison of theoretical and simulated output waveforms. (a) 600 ns. (b) 60 ns.

III. FAULT FEATURE IN CONDITION OF SINGLE-END TEST

A. CALCULATION OF THE ILI

According to the impedance matrix in (14), the scattering matrix (S matrix) can be calculated as [37]

$$S_T = \begin{bmatrix} S_{11} & S_{12} \\ S_{21} & S_{22} \end{bmatrix} = \left(Z_T Z_{port}^{-1} + Z_{port}\right)^{-1} \left(Z_T Z_{port}^{-1} - Z_{port}\right), \quad (17)$$

where $Z_{port} = \begin{bmatrix} \sqrt{R_s} & 0 \\ 0 & \sqrt{R_L} \end{bmatrix}$.

The element S_{21} in the S matrix is generally referred to as the insertion loss (IL). According to the definition of the S matrix, in essence, the IL is the ratio of the square root of power between the output waveform in port 2 and input waveform in port 1. According to (17), it is calculated as

$$S_{21} = \frac{2\sqrt{R_s R_L}}{R_s A_{22} + A_{11} R_L + R_s A_{21} R_L + A_{12}}. \quad (18)$$

Equation (18) can be reduced to

$$S_{21} = \frac{2Z_0\sqrt{\Gamma_s\Gamma_L}}{\eta_1 Z_C + \eta_2 Z_0}. \quad (19)$$

With the new contact impedance Z'_C, the IL is calculated as

$$S'_{21} = \frac{2Z_0\sqrt{\Gamma_s\Gamma_L}}{\eta_1 Z'_C + \eta_2 Z_0}. \quad (20)$$

The new IL S'_{21} can be expressed by the old IL S_{21}

$$S'_{21} = \frac{\eta_1 Z_C + \eta_2 Z_0}{\eta_1 Z'_C + \eta_2 Z_0} S_{21}. \quad (21)$$

We convert the unit of the new IL into decibel (dB) to obtain

$$IL'_{21} = 10\log_{10}(|S'_{21}|) = 10\log_{10}\left(\left|\frac{\eta_1 Z_C + \eta_2 Z_0}{\eta_1 Z'_C + \eta_2 Z_0}\right|\right) + 10\log_{10}(|S_{21}|) = 10\log_{10}\left(\left|\frac{\eta_1 Z_C + \eta_2 Z_0}{\eta_1 Z'_C + \eta_2 Z_0}\right|\right) + IL_{21}. \quad (22)$$

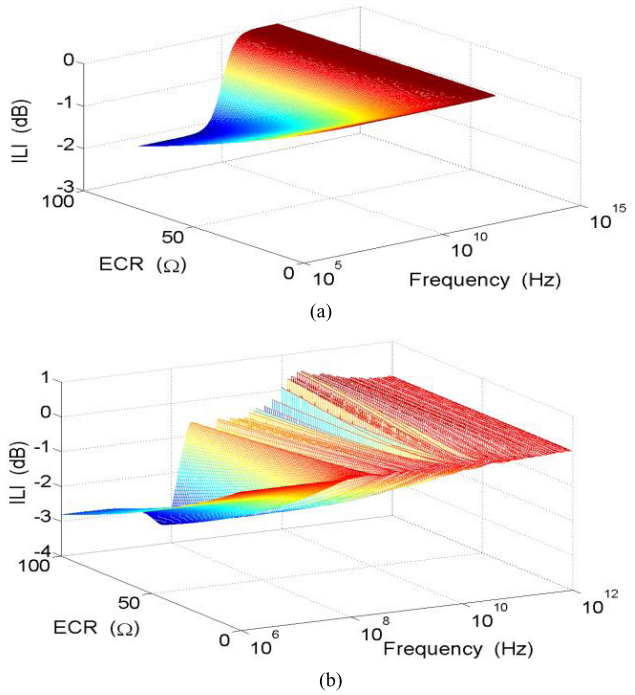

FIGURE 6. ILI results varying with ECR and frequency. (a) Impedance matching. (b) Impedance mismatching.

Thus, according to (22), the insertion loss increment (ILI) between the new and old contact state is estimated as

$$\delta_{IL} = IL'_{21} - IL_{21} = 10\log_{10}\left(\left|\frac{\eta_1 Z_C + \eta_2 Z_0}{\eta_1 Z'_C + \eta_2 Z_0}\right|\right). \quad (23)$$

In view of the last equation, the ILI has correlation with the change of contact impedance. As shown in Fig. 1, the contact impedance is made up of ECR and ECC.

The ECC is of the order of several pico-farads at magnitude [38]. For example, Deutsch *et al.* [39] indicated that the mean value of capacitance was 1.9 pF for a pinned connector and varied from 1.86 to 1.99 pF for a pad-on-pad connector. According to Kwiatkowski *et al.* [40], the ECC is 2.57 pF for a typical electro-mechanical switch, 0.1417 pF for a typical RF MEMS switch and 1.72 fF for an open path. Generally, the impact of the ECC is remarkable only when the frequency is particularly high. Moreover, the larger the capacitance is, the more significant the impact will be. However, the ECC will rapidly decrease in the degradation process. When the intermittence is active, the ECC is miniscule and can even be neglected. With no loss of generality, the ECC is set as 20 pF in the normal contact state and 200 fF in the fault contact state.

For example, the parameters are set as follows: $R_C = 0.01\Omega$, $Z_0 = 75\ \Omega$, $C_C = 20$ pF, $C'_C = 200$ fF, $t_{d1} = 1.086$ ns, and $t_{d2} = 2.172$ ns. When in both the source and load ends the impedances are matching ($R_s = R_L = Z_0$) or mismatching ($R_s = 10\ \Omega$, $R_L = 100\ \Omega$), the ILI results will vary with the signal frequency and the ECR, as shown in Fig. 6. This figure indicates that the smaller the signal frequency is and the higher the ECR is, the greater the absolute value of ILI will be.

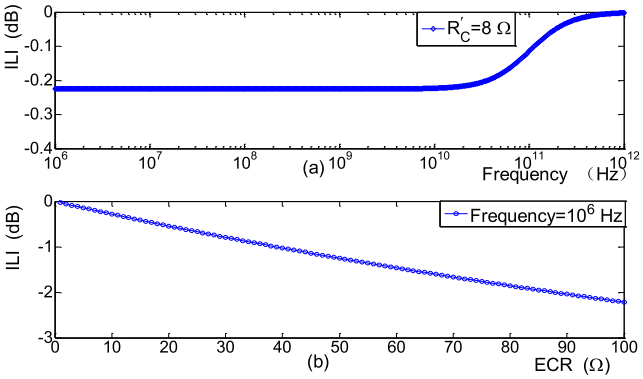

FIGURE 7. ILI curves varying with (a) Signal frequency. (b) ECR.

In case of fixing the ECR value or the signal frequency, the absolute value of ILI will increase with decrease of signal frequency or increase of ECR, respectively, as shown in Fig. 7. Furthermore, the ILI curve can remain constant below a considerably high frequency (higher than 10 GHz in this case). When the bandwidth of the transmitted signal is smaller than the highest frequency below which the ILI is stable, the stationary ILI value can be taken as the fault threshold, which corresponds to the ECR threshold. For most connectors between devices in the electromechanical system, this condition can be satisfied.

B. ILI MEASUREMENT

In view of the physical meaning of IL, the ILI can be estimated as

$$\begin{aligned}\delta_{IL} &= 10\log_{10}\left(\sqrt{\frac{P'_{out}}{P'_{in}}}\right) - 10\log_{10}\left(\sqrt{\frac{P_{out}}{P_{in}}}\right)\\ &= 10\log_{10}\sqrt{P'_{out}} - 10\log_{10}\sqrt{P_{out}}\\ &\quad - (10\log_{10}\sqrt{P'_{in}} - 10\log_{10}\sqrt{P_{in}}), \end{aligned} \quad (24)$$

where P'_{out} and P_{out} are the mean powers of the received signal in the new and old contact states, respectively. The variables P'_{in} and P_{in} are the mean powers of the sent signal in the new and old contact states, respectively. The high level and low level voltages are determinate for the digital signal, so there will be $P'_{in} = P_{in}$. Accordingly, the measured value of ILI can be expressed as

$$\delta_{IL} = 10\log_{10}\sqrt{P'_{out}} - 10\log_{10}\sqrt{P_{out}}. \quad (25)$$

According to (25), the discrete ILI sequence can be obtained by only measuring the voltage at the receiver end. For a discrete voltage sequence $v(n)$ with the size of N_v, the corresponding discrete Fourier transform is denoted as $F(k)$, and then the power of the voltage sequence can be computed as

$$P = \frac{1}{N_v}\sum_{n=0}^{N-1}|v(n)|^2 = \frac{1}{N_v^2}\sum_{k=0}^{N-1}|F(k)|^2. \quad (26)$$

If it is required to detect the intermittence that is lasting for more than T_A seconds, the voltage sample frequency F_s will be

$$F_s = N_v F_d = N_v / T_A, \tag{27}$$

where F_d is the detection frequency. The larger the sequence size N_v is, the more accurate the calculation of the power will be, but the higher the voltage sample frequency will be. So the sequence size should be set appropriately. Accordingly, the electrical connector IF can be detected in real time.

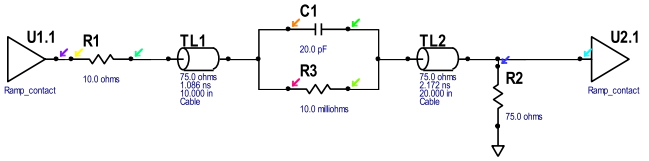

FIGURE 8. HyperLynx simulation model for ILI measurement.

C. COMPARISON OF MODEL AND SIMULATION RESULTS OF ILI

To verify the ILI model, a HyperLynx simulation model of the circuit in Fig. 2 was developed, which can be employed for the SI analysis. The ILI values measured from the simulated output waveform are compared with the model values in (23). The HyperLynx model is shown in Fig. 8. The parameters are set as below. The time delays are 1.086 ns and 2.172 ns for the first and the second transmission lines, respectively. The characteristic impedances of the two transmission lines are 75 Ω. In the normal contact state, the ECR R_C is 0.01 Ω, and the ECC C_C is 20 pF, while in the abnormal contact state, the ECR R'_C values are set respectively as 8 Ω and 50 Ω, and the ECC C'_C is 200 fF. The sent signal is a square waveform with a frequency of 1 MHz, amplitude of 1 V, rise time of 2 ns, and duty ratio of 50%. Four different cases are considered:

Case 1: Impedances in both the source and load ends are matching. Let $R_s = R_L = 75\ \Omega$.

Case 2: Impedances in the source end are matching. Let $R_s = 75\ \Omega$ and $R_L = 100\ \Omega$.

Case 3: Impedances in the load end are matching. Let $R_s = 10\ \Omega$ and $R_L = 75\ \Omega$.

Case 4: Impedances in both the source and load ends are mismatching. Let $R_s = 10\ \Omega$ and $R_L = 100\ \Omega$.

The ILI comparison results are shown in Table 1. These results indicate that the errors between model values and simulation values are smaller than 1%. This comparison indicates the validity of the ILI model.

IV. ILI-BASED CONNECTOR IF ON-LINE DIAGNOSIS METHOD

By comparing the voltage waveform at the receiver end to the threshold voltages of high and low levels, the ECR fault threshold can be determined. According to the ECR fault threshold, the ILI fault threshold can be calculated via (23). As shown in Fig. 9, the ILI curve will have a negative pulse

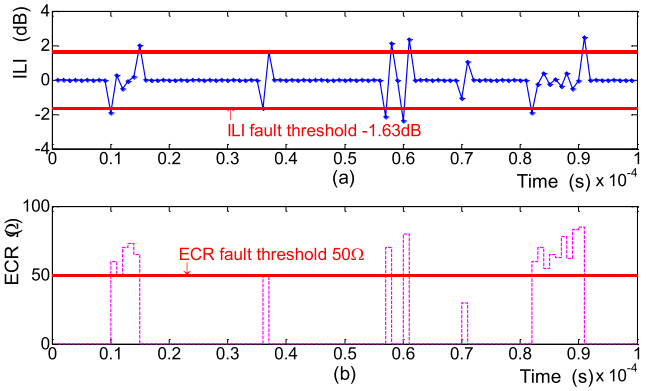

FIGURE 9. Detection of the IF according to (a) ILI curve. (b) ECR curve.

when the IF turns into activity or a positive pulse when the IF turns into inactivity. When the connector has an IF, the ECR will change sharply under environmental stresses, especially under the vibration stress. Therefore, the IF activity and inactivity will appear alternately, and the same is true for the negative and positive pulses in the ILI curve. Thus, the activity time will be the distance between the adjacent negative pulse and positive pulse, both of which are exceeding the ILI threshold. The activity time is estimated as

$$T_A^{(i)} = t_i^{e+} - t_i^{e-}, \tag{28}$$

where $T_A^{(i)}$ is the ith IF activity time, t_i^{e-} is the time at which the ith negative pulse exceeds the threshold, and t_i^{e+} is the time at which the ith positive pulse exceeds the threshold. Considering Case 4 in Table 1, the ECR sequence is shown in Fig. 9(b), and the corresponding ILI curve and fault threshold are shown in Fig. 9(a). The comparison of the ILI and ECR curves illustrates that the IF can be detected exactly according to the ILI curve.

TABLE 1. Comparison of model and simulation results of ILI.

Impedance match case	ECR (Ω)	Model ILI (dB)	Simulated ILI (dB)	Error
Case 1	8	-0.2254	-0.2254	0.00676%
Case 1	50	-1.2491	-1.2488	0.0257%
Case 2	8	-0.1942	-0.1955	0.67%
Case 2	50	-1.0930	-1.0992	0.58%
Case 3	8	-0.3897	-0.3867	0.78%
Case 3	50	-2.0071	-1.9916	0.77%
Case 4	8	-0.3055	-0.3077	0.73%
Case 4	50	-1.6396	-1.6315	0.50%

The ILIs represent the IL variations between the adjacent contact states. Therefore, when the ECR increases slowly, decreases slowly or fluctuates during different fault states, the ILI may not exceed the fault threshold, but in fact the fault is active. Thus, according to (28), the fault activity may not be detected. As shown in Fig. 10(b), the first and third fault activities will be undetected, as their corresponding ILI values do not exceed the fault threshold. In view of this, the decision method should be modified. Assume that the contact impedance corresponding to the contact state sequence

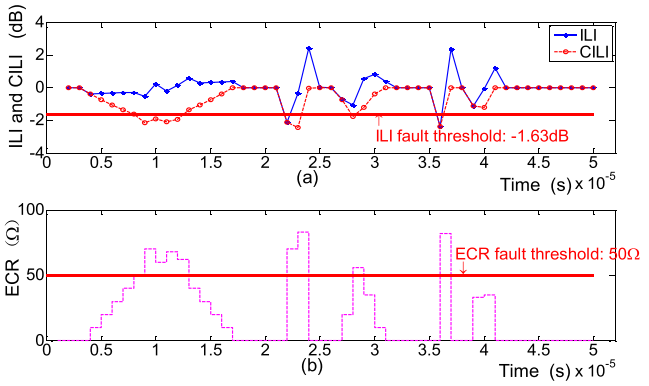

FIGURE 10. Detection of IF according to (a) CILI curve. (b) ECR curve.

$\{S_i|i = 1, 2, \ldots, N\}$ is denoted as $\{Z_C^i|i = 1, 2, \ldots, N\}$. Thus, according to (23), the corresponding ILI $\{\delta_{IL}^i|i = 2, \ldots, N\}$ can be calculated as

$$\delta_{IL}^i = 10\log_{10}\left(\left|\frac{\eta_1 Z_C^{i-1} + \eta_2 Z_0}{\eta_1 Z_C^i + \eta_2 Z_0}\right|\right). \tag{29}$$

Therefore, the summation of the ILI sequence will be

$$\begin{aligned}
&\delta_{IL}^2 + \delta_{IL}^3 + \cdots + \delta_{IL}^N \\
&= 10\log_{10}\left(\left|\frac{\eta_1 Z_C^1 + \eta_2 Z_0}{\eta_1 Z_C^2 + \eta_2 Z_0}\right|\right) + 10\log_{10}\left(\left|\frac{\eta_1 Z_C^2 + \eta_2 Z_0}{\eta_1 Z_C^3 + \eta_2 Z_0}\right|\right) \\
&\quad + \cdots + 10\log_{10}\left(\left|\frac{\eta_1 Z_C^{N-1} + \eta_2 Z_0}{\eta_1 Z_C^N + \eta_2 Z_0}\right|\right) \\
&= 10\log_{10}\left(\left|\frac{\eta_1 Z_C^1 + \eta_2 Z_0}{\eta_1 Z_C^N + \eta_2 Z_0}\right|\right) \\
&= \delta_{IL}^{(N,1)}.
\end{aligned} \tag{30}$$

Equation (30) indicates that the ILI value between two contact states equals the summation of the ILI values of the refinement states between the two contact states. The symbol "1" in $\delta_{IL}^{(N,1)}$ denotes the initial contact state, so $\delta_{IL}^{(N,1)}$ represents the ILI value between the present and the initial contact state. As $\delta_{IL}^{(N,1)}$ is the summation of all historical ILI values, it is referred to as the cumulative insertion loss increment (CILI), which is simply denoted as δ_{CIL}^N.

Furthermore, the ECR corresponding to the initial CILI value may not be the minimum. When the ECR is larger than its initial value, the CILI should be greater than 0 dB. Hence, the CILI curve should be translated downward to smaller than 0 dB. The new CILI is estimated as

$$\tilde{\delta}_{CIL}^i = \delta_{CIL}^i - Max(\{\delta_{CIL}^i\}). \tag{31}$$

The IF can be detected according to the CILI. When it satisfies

$$\tilde{\delta}_{CIL}^N \le \delta_{th}, \tag{32}$$

then the fault is active. In this equation, δ_{th} is the ILI fault threshold. The CILI sequence obtained from continuous measuring forms the fault feature curve. In Fig. 10(a), the ILI and CILI curves are displayed. By comparing those curves to the ECR curve in Fig. 10(b), it is apparent that when the ECR slowly increases to above the threshold, the ILI may still not exceed the fault threshold, while the CILI exceeds the fault threshold. Thus, the IF can be exactly detected according to the CILI.

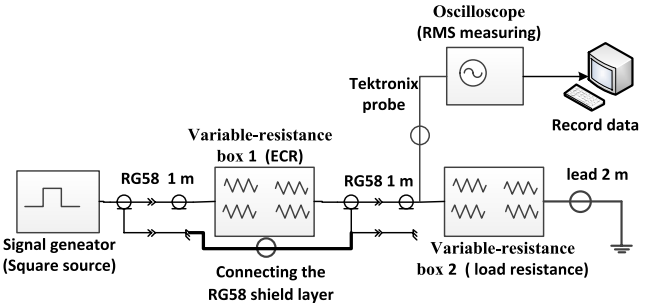

FIGURE 11. ILI measurement diagram under the determinate ECR.

When the minimum value Z_C^m of the contact impedance sequence $\{Z_C^i|i = 1, 2, \ldots, N\}$ deviates from the normal impedance Z_C^b, the computation of CILI will has an error, which can be estimated as

$$\tilde{\delta}_{CIL}^e = 10\log_{10}\left(\left|\frac{\eta_1 Z_C^b + \eta_2 Z_0}{\eta_1 Z_C^m + \eta_2 Z_0}\right|\right). \tag{33}$$

Because Z_C^m is unknown, the error cannot be worked out. However, during a long-time measurement, the minimum contact impedance is generally regarded as a value in normal state. Therefore, the error can be neglected.

V. VERIFICATION OF ILI-BASED ON-LINE DIAGNOSIS METHOD FOR ELECTRICAL CONNECTOR IF

As the application situation of the proposed diagnosis method is different from current approaches, so this method will be verified by both qualitative and quantitative approaches, which are according to the experimental results.

A. QUALITATIVE VERIFICATION

Connected in tandem into the cables, the variable-resistance boxes are used to produce the contact and load resistances. The test diagram is shown in Fig. 11. An Agilent 33220A type signal generator sent out a square signal with frequency of 1 MHz, high level voltage of 3.3 V, and low level voltage of −3.3 V. The transmission lines were RG58 cables with a length of 1 m and characteristic impedance of 50 Ω. A Tektronix MSO2024B oscilloscope was used to measure the signal at the receiver end. A computer was connected to the oscilloscope to record the measurement results.

In the test, the sample frequency of the oscilloscope is 1 GHz. The connector IF with a length of a signal period, which is one microsecond, is demanded to detect, so the sequence size N_v is set as 1000. The voltage root mean square (RMS) value in a period was measured every second by using the toolbox provided by the oscilloscope manufacturer. The signal power, ILI and CILI are then calculated from the RMS results.

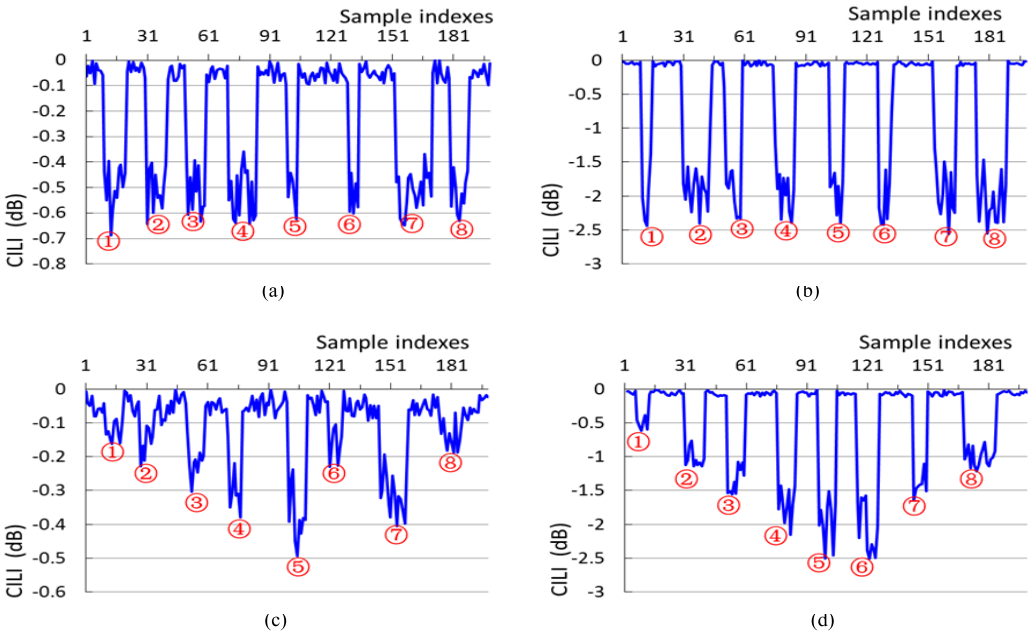

FIGURE 12. CILI (load resistance of 1000 Ω) under different ECR groups. (a) Group 1. (b) Group 2. (c) Group 3. (d) Group 4.

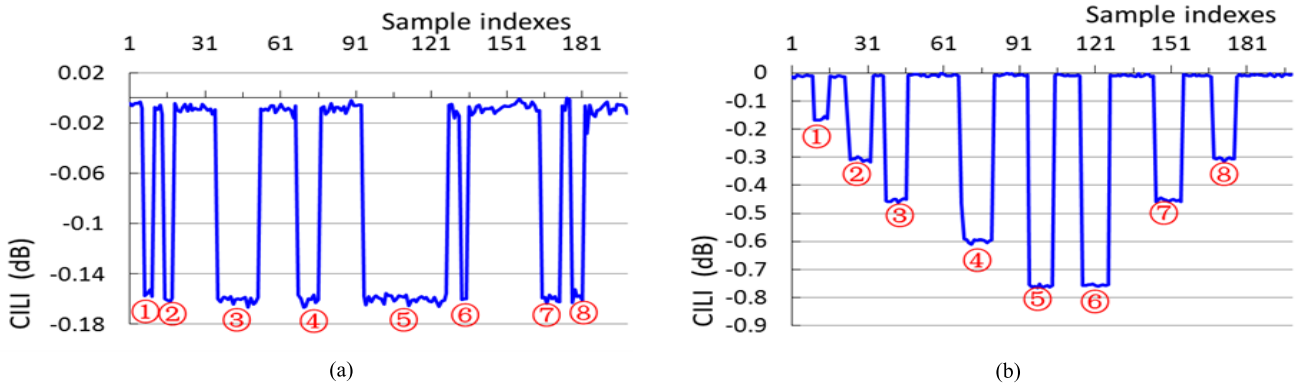

FIGURE 13. CILI (ungrounded) under different ECR groups. (a) Group 1. (b) Group 4.

TABLE 2. Settings of the variable-resistance box.

Group No.	Variable-resistance box value (Ω)							
	Value 1	Value 2	Value 3	Value 4	Value 5	Value 6	Value 7	Value 8
Group 1	100	100	100	100	100	100	100	100
Group 2	500	500	500	500	500	500	500	500
Group 3	20	40	50	60	80	40	70	30
Group 4	100	200	300	400	500	500	300	200

To compare the variations of the ECR and CILI, the variant-resistance box was shifted manually to produce different ECRs. Four abnormal ECR groups with a sample size of 8 were tested, as shown in Table 2. In each test group, 200 RMS values were measured.

When the load resistance is 1000 Ω, the CILI curves of different ECR groups are shown in Fig. 12. The CILI accidents, which are corresponding to the sudden changes of ECR, are marked out. This figure illustrates that the CILI curve will have accidents when the ECR increases. Moreover, the greater the ECR deviation is, the more significant the CILI accident will be. This qualitative test demonstrates that the CILI can exhibit the variation of the ECR.

The CILI curves in Fig. 12 have considerable noises. This result is mainly due to the imperfect grounding. The grounding voltage was found to be as high as 1 V. When the load resistance increases, the grounding noise will be inhibited. In fact, when the load resistance was 100 Ω, the noises were more conspicuous. When the experimental circuit was floating, CILI noises were much smaller, and the CILI accidents were consistent with the sharp ECR variations, as shown in Fig. 13.

However, for the electrical connector with an IF, it is still unknown how the CILI would change under vibration

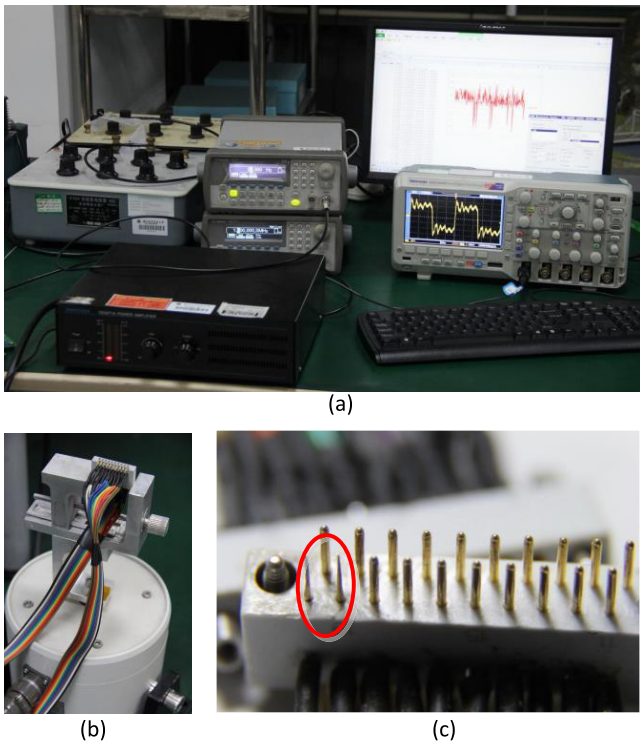

FIGURE 14. ILI measuring pictures under vibration stress. (a) Assembly picture. (b) Vibrator. (c) Fault injection.

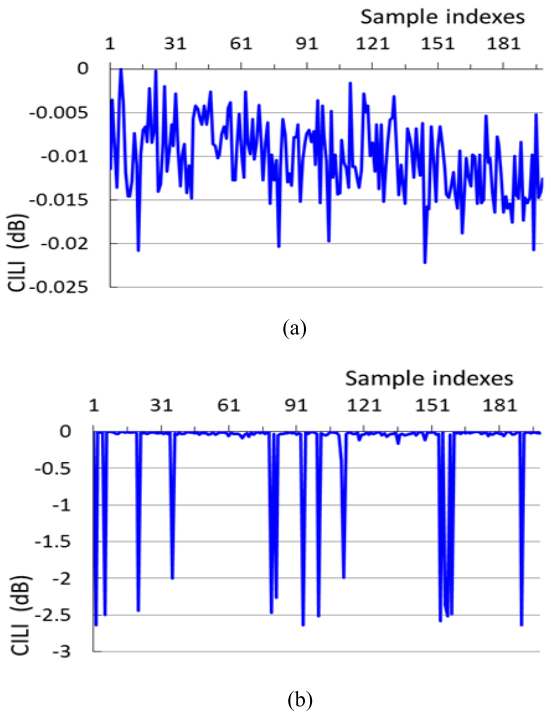

FIGURE 15. Comparison of the CILI under (a) No vibration. (b) Vibration with frequency of 20 Hz.

stress. Therefore, in the following experiment, a JONHON CY1T20WJ-CY1Z20HJ type connector was tested instead of the variant-resistance box. As marked in the Fig. 14(c), two pins of the electrical connector were milled thinner. Accordingly, the contact pairs were not contact well. Thus the IFs would take place under vibration stress. The connector was then fixed on a minitype vibrator.

The signal generator supplied a sinusoidal voltage signal with amplitude of 2 V to the power amplifier that can transform the voltage signal to current signal to drive the vibrator. The output current can be regulated to as high as 10 A. In the test, the gain of the power amplifier was adjusted to a level to produce proper intensity of vibration. In condition of fixed current gain, the smaller the vibration frequency is, the greater the vibration displacement will be. Several measurements under different vibration frequency were carried out. It was found that the vibration displacement was adequate when the vibration frequency was 20 Hz. So the case when the vibrator produced sinusoidal vibration with frequency of 20 Hz was taken as the example.

The CILI curve is shown in Fig. 15(b). For the purpose of comparison, the CILI curve under no vibration is also shown in Fig. 15(a). The comparison indicates that when the vibration stress is loaded on the connector, the IF will be active or inactive alternately, and the CILI will have significant accidents. These findings demonstrate the applicability of the CILI for detecting connector IFs.

B. QUANTITATIVE VERIFICATION

To quantitatively verify the ILI-based IF diagnosis method of the electrical connector, the circuit parameters should be determined, and the ECR and ILI should be measured synchronously. In the following, the Simulink model for the transmission circuit is built up. In this model, the ECRs are from the measured data in the vibration experiments. The ILIs are calculated according to the simulation output waveforms. The IF activities are then detected according to (32).

The four-wire resistance measuring method was used to measure the ECR. Thus, the lead resistance of the measurement loop can be eliminated to obtain a precise ECR. There were two loop circuits connected to the contact pair. A constant current of 0.3 A was passed through one circuit, while the voltage drop of the contact was sampled in the other circuit via a data acquisition (DAQ) board, whose type was art-control PCI-8504. The sampling frequency was 4 MHz. The sampling resolution was 2 mΩ, and the measurement range was from 0 to 16.66 Ω. The test rig is shown in Fig. 16.

The Simulink model of the transmission circuit is shown in Fig. 17. The involved parameters are set as those of Case 4 in Table 1. This model includes four functional modules, i.e., the signal source, transmission channel, ILI measurement and error rate analysis. As the maximum range of the DQA board is only 16.66 Ω, no loss of generality, the ECR fault threshold is set as 8 Ω. The corresponding ILI fault threshold is then calculated to be −0.3055 dB.


(a)

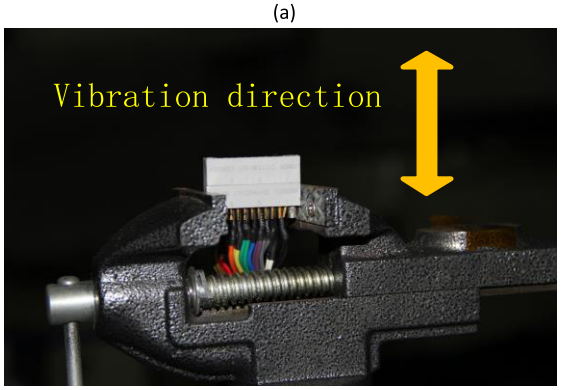

(b)

FIGURE 16. Assembly picture. (a) ECR measurement board. (b) connector.

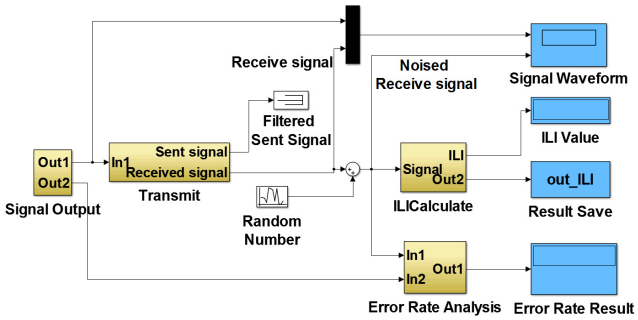

FIGURE 17. Simulink model for the transmission circuit.

Regarding the measurement result with a sample size of 5000, the CILI and ECR curves are shown in Fig. 18. The parameter architecture for characterizing the IF has been proposed in the previous work of the authors [41]. Herein, the parameters are calculated from the diagnosis results. The IF activity probability is the probability that the IF is active when IF is present. The IF activity time is the duration time of an IF activity. The IF inactivity probability is the probability that the IF is inactive when IF is present. The IF inactivity time is the duration time of an IF inactivity. The IF quantity is the number of activities in a limited time. The IF frequency is the IF activity number per unit time. Pseudo-period is the average time of the cycle of IF activities.

The evaluation results of the parameters are shown in Table 3. The errors between the diagnosis results and the real results calculated from the ECR are very small. In the

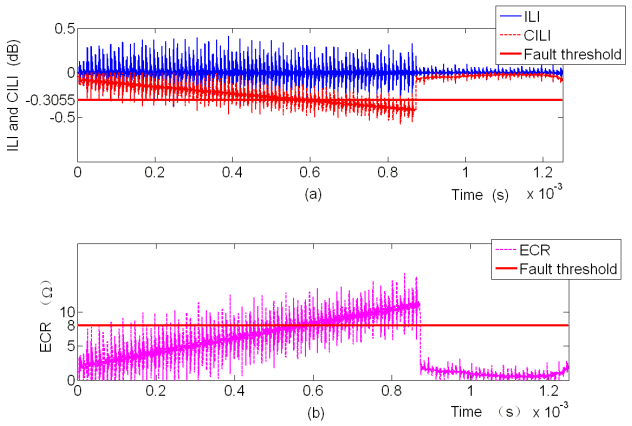

FIGURE 18. IF diagnosis results according to (a) CILI. (b) ECR.

TABLE 3. Comparison of IF parameters.

Result from	Samples exceed threshold	IF activity probability	IF activity time (μs)	IF inactivity probability	IF inactivity time (μs)	IF quantity	IF frequency	Pseudo -period (μs)
ECR	1230	0.2460	0.9762	0.7540	2.9826	315	252000	3.9683
Diagnosis	1223	0.2446	0.9615	0.7554	2.96	318	254400	3.9308
Error	0.57%	0.57%	1.51%	0.19%	0.76%	0.95%	0.95%	0.94%

TABLE 4. The ECR corresponding to the undetected IF activities.

Sample positions	2193	2349	2379	2391	2462	2562	3051
ECR(Ω)	8.006	8.020	8.022	8.020	8.014	8.016	8.020

diagnosis, only 7 samples above the ECR fault threshold are not detected. These undetected fault samples would break down some IF activities and result in increase of the IF quantity. The indexes of undetected fault samples and the corresponding resistance values are shown in Table 4. The table illustrates that the resistances of the undetected faults are only a little greater than the ECR threshold. In fact, when the ILI threshold is set as -0.305 dB, whose absolute value is appreciably lower than -0.3055 dB, only the fault activity with a resistance of 8.006 Ω is not detected. The quantitative results show that the ILI-based on-line diagnosis method for the connector IF can detect the IF effectively. The error is less than 1%.

VI. CONCLUSION

In this paper, the impact of ECR on the high-speed signal transmission performance has been analyzed in frequency and time domain respectively. The model of ILI which is taken as the fault feature in condition of single-end test has been developed. After that the ILI-based on-line diagnosis method for electrical connector intermittent faults is proposed. The qualitative and quantitative tests have verified the applicability of the proposed method. The verification shows that the errors of IF parameters are less than 1%.

The proposed ILI-based diagnosis method merely requires the measurement of the output voltage signal of the electrical

connector. Thus, this method does not require additional measurement paths and will be applicable for the built-in test. Consequently, the intermittent faults in the large-scale electrical connectors can be detected in real time. In a word, the study in this paper provides an approach to solve the troublesome problem of electrical connector intermittent fault.

VII. Acknowledgment

Q. Shen and K. Lv contributed equally to this work.

REFERENCES

[1] B. A. Sorensen, G. Kelly, A. Sajecki, and P. W. Sorensen, "An analyzer for detecting intermittent faults in electronic devices," in *Proc. IEEE Syst. Readiness Technol. Conf. (AUTOTESTCON)*, Anaheim, CA, USA, 1994, pp. 417–421.

[2] W. A. Syed, S. Khan, P. Phillips, and S. Perinpanayagam, "Intermittent fault finding strategies," in *Proc. CIRP*, 2013, pp. 74–79.

[3] B. Steadman, F. Berghout, N. Olsen, and B. Sorensen, "Intermittent fault detection and isolation system," in *Proc. AUTOTESTCON*, Salt Lake, UT, USA, 2008, pp. 37–40.

[4] B. Steadman, L. S. Sievert, B. Sorensen, and F. Berghout, "Attacking 'bad actor' and 'no fault found' electronic boxes," in *Proc. AUTOTESTCON*, Orland, FL, USA, 2005, pp. 821–824.

[5] H. Wu, "Reliability modeling and statistical verification for space electrical connector under combined stress," M.S. thesis, College Mech. Energy Eng., Zhejiang Univ., Hangzhou, China, 2007.

[6] W. H. Abbott, "Time distribution of intermittents versus contact resistance for tin-tin connector interfaces during low amplitude motion," *IEEE Trans. Compon., Hybrids, Manuf. Technol.*, vol. 7, no. 1, pp. 107–111, Mar. 1984.

[7] S. R. Murrell and S. L. McCarthy, "Intermittence detection in fretting corrosion studies of electrical contacts," in *Proc. 43rd IEEE Holm Conf. Elect. Contacts*, Philadelphia, PA, USA, Oct. 1997, pp. 1–6.

[8] C. Maul and J. W. McBride, "A model to describe intermittency phenomena in electrical connectors," in *Proc. 48th IEEE Holm Conf. Elect. Contacts*, Orlando, Florida, Oct. 2002, pp. 165–174.

[9] A. F. Anderson, "Intermittent electrical contact resistance as a contributory factor in the loss of automobile speed control functional integrity," *IEEE Access*, vol. 2, pp. 258–289, 2014.

[10] H. Qi, S. Ganesan, and M. Pecht, "No-fault-found and intermittent failures in electronic products," *Microelectron. Rel.*, vol. 48, no. 5, pp. 663–674, May 2008.

[11] E. M. Bock and J. H. Whitley, "Fretting corrosion in electric contacts," in *Proc. 20th IEEE Holm Conf. Elect. Contacts*, Chicago, IL, USA, Oct. 1974, pp. 128–138.

[12] M. Antler, "Effect of fretting on the contact resistance of palladium electroplate having a gold flash, cobalt-gold electroplate, and DG R156," in *Proc. 34th Electron. Compon. Conf.*, New Orleans, LA, USA, 1984, pp. 343–350.

[13] M. Antler, "Survey of contact fretting in electrical connectors," *IEEE Trans. Compon., Hybrids, Manuf. Technol.*, vol. 8, no. 1, pp. 87–104, Mar. 1985.

[14] N. Aukland, I. Leslie, H. Hardee, and P. Lees, "A statistical comparison of a clad material and gold flashed palladium-nickel under various fretting conditions," in *Proc. 41st IEEE Holm Conf. Elect. Contacts*, Montreal, QC, Canada, Oct. 1995, pp. 52–63.

[15] J. Swingler and J. W. McBride, "Fretting corrosion studies of an extrinsic conducting polymer and tin interface," in *Proc. 47th IEEE Holm Conf. Elect. Contacts*, Montreal, QC, Canada, Sep. 2001, pp. 215–219.

[16] R. D. Malucci, "Characteristics of films developed in fretting experiments on tin plated contacts," in *Proc. 45th IEEE Holm Conf. Elect. Contacts*, Pittsburg, CA, USA, Oct. 1999, pp. 175–185.

[17] M. D. Bryant, "Resistance buildup in electrical connectors due to fretting corrosion of rough surfaces," *IEEE Trans. Compon., Packag., Manuf. Technol., A*, vol. 17, no. 1, pp. 86–95, Mar. 1994.

[18] G. T. Flowers, F. Xie, M. J. Bozack, R. Horvath, R. D. Malucci, and B. I. Rickett, "Modeling early stage fretting of electrical connectors subjected to random vibration," in *Proc. 49th IEEE Holm Conf. Elect. Contacts*, Dec. 2003, pp. 45–50.

[19] G. T. Flowers, F. Xie, M. J. Bozack, and R. D. Malucci, "Vibration thresholds for fretting corrosion in electrical connectors," *IEEE Trans. Compon. Packag. Technol.*, vol. 27, no. 1, pp. 65–71, Mar. 2004.

[20] D. Skinner, "Intermittent opens in electrical contacts caused by mechanically induced contact motion," *IEEE Trans. Parts, Hybrids, Packag.*, vol. 11, no. 1, pp. 72–76, Mar. 1975.

[21] R. D. Malucci, "Possible mechanism for observed dynamic resistance," in *Proc. 46th IEEE Holm Conf. Elect. Contacts*, Chicago, IL, USA, Sep. 2000, pp. 254–267.

[22] J. W. McBride, "The relationship between surface wear and contact resistance during the fretting of *in-vivo* electrical contacts," *IEEE Trans. Compon. Packag. Technol.*, vol. 31, no. 3, pp. 592–600, Sep. 2008.

[23] C. Maul, J. W. McBride, and J. Swingler, "Intermittency phenomena in electrical connectors," *IEEE Trans. Compon. Packag. Technol.*, vol. 24, no. 3, pp. 370–377, Sep. 2001.

[24] S. B. Smith, V. Balasubramanian, D. Nardone, and S. S. Agili, "Effect of nanosecond electrical discontinuities in high-speed digital applications," in *Proc. 54th IEEE Holm Conf. Elect. Contacts*, Oct. 2008, pp. 47–52.

[25] Y. Chen and S. Baisheng, "Investigate the influence of contact impedance on digital signal transmission by computer simulation method," in *Proc. 49th IEEE Holm Conf. Elect. Contacts*, Sep. 2003, pp. 29–37.

[26] R. D. Malucci, "The impact of contact resistance on high speed digital signal transmission," in *Proc. 48th IEEE Holm Conf. Elect. Contacts*, Oct. 2002, pp. 212–220.

[27] W. G. Zanardelli, E. G. Strangas, and S. Aviyente, "Identification of intermittent electrical and mechanical faults in permanent-magnet AC drives based on time–frequency analysis," *IEEE Trans. Ind. Appl.*, vol. 43, no. 4, pp. 971–980, Jul./Aug. 2007.

[28] S. S. H. Zaidi, W. G. Zanardelli, S. Aviyente, and E. G. Strangas, "Comparative study of time-frequency methods for the detection and categorization of intermittent faults in electrical drives," in *Proc. Int. Symp. Diagnostics Elect. Mach., Power Electron. Drives (SDEMPED)*, Sep. 2007, pp. 39–45.

[29] M. M. Alamuti, H. Nouri, R. M. Ciric, and V. Terzija, "Intermittent fault location in distribution feeders," *IEEE Trans. Power Del.*, vol. 27, no. 1, pp. 96–103, Jan. 2012.

[30] A. Yaramasu, Y. Cao, G. Liu, and B. Wu, "Intermittent wiring fault detection and diagnosis for SSPC based aircraft power distribution system," in *Proc. IEEE/ASME Int. Conf. Adv. Intell. Mech.*, Kaohsiung, Taiwan, Jul. 2012, pp. 1117–1122.

[31] M. Ballas, N. Locken, C. Parkey, and C. Hughes, "A non-destructive high-voltage low-energy intermittent fault location system," in *Proc. IEEE AUTOTESTCON*, Sep. 2011, pp. 78–86.

[32] S. A. Artishchev and E. V. Semyonov, "Method for the detection of small defects of electrical contacts by thermononlinear reflectometry with compensation of non-invariance of test signal's generator," in *Proc. 23rd Int. Crimean Conf. Microw. Telecommun. Technol.*, Sep. 2013, pp. 1018–1019.

[33] L. Boyer, F. Houze, G. Klimek, and S. Noel, "Electrical and physical modeling of contact defects due to fretting," *IEEE Trans. Compon., Packag., Manuf. Technol., A*, vol. 17, no. 1, pp. 134–140, Mar. 1994.

[34] G. Geurts, A. Wiekamp, and E. VanderHeyden, "Modern connector design tools assure high speed signal integrity," in *Proc. 45th Electron. Compon. Technol. Conf.*, May 1995, pp. 154–160.

[35] R. Achar and M. S. Nakhla, "Simulation of high-speed interconnects," *Proc. IEEE*, vol. 89, no. 5, pp. 693–728, May 2001.

[36] S. H. Hall and H. L. Heck, *Advanced Signal Integrity for High-Speed Digital Designs*. Hoboken, NJ, USA: Wiley, 2009.

[37] B. Young, *Digital Signal Integrity: Modeling and Simulation With Interconnects and Packages*. Upper Saddle River, NJ, USA: Prentice-Hall, 2001.

[38] G. F. Dorsey, D. S. Coleman, and B. K. Witherspoon, "High speed data across sliding electrical contacts," in *Proc. IEEE 58th Holm Conf. Elect. Contacts*, Sep. 2012, pp. 1–12.

[39] A. Deutsch *et al.*, "Electrical characteristics of high-performance pin-in-socket and pad-on-pad connectors," *IEEE Trans. Compon., Packag., Manuf. Technology, Part B*, vol. 20, no. 1, pp. 64–77, Feb. 1997.

[40] R. Kwiatkowski, M. Vladimirescu, A. Zybura, and S. Choi, "Scattering parameter model of low level electrical contacts in electro-mechanical microwave switches-a switch manufacturer approach," in *Proc. 49th IEEE Holm Conf. Elect. Contacts*, Oct. 2002, pp. 221–230.

[41] Q. Shen, J. Qiu, G. Liu, and K. Lv, "Intermittent faults parameter framework and stochastic Petri net based formalization model," *Eksploatacja Niezawodnosc Maintenance Rel.*, vol. 18, no. 2, pp. 210–217, Apr. 2016, doi: 10.17531/ein.2016.2.8.

QINMU SHEN received the B.S. degree from Zhejiang University in 2005 and the M.S. degree from the National University of Defense Technology in 2008, where he is currently pursuing the Ph.D. degree with the College of Mechatronic Engineering and Automation. His areas of research include design for testability, fault diagnosis, and signal integrity analysis.

KEHONG LV received the B.S. degree from Xi'an Jiaotong University in 2001, and the M.S. degree and the Ph.D. degree in mechatronic engineering from the National University of Defense Technology (NUDT) in 2003 and 2008, respectively. Since 2008, he has been with NUDT, where he is currently a Vice-Professor of Mechanical Engineering. His current research interests include prognostics and health management, design for testability, built-in test, mechanical signal processing and data fusion, condition monitoring, and fault diagnosis.

GUANJUN LIU received the B.S. and Ph.D. degrees in mechanical engineering from the National University of Defense Technology (NUDT) in 1994 and 2000, respectively. Since 2000, he has been with NUDT, where he is currently a Professor and a Ph.D. Supervisor of Mechanical Engineering. He has authored over 100 articles, primarily in condition monitoring, fault diagnosis techniques, and the technology of decreasing false alarms. His research interests include fault diagnosis, testability, and maintenance.

JING QIU received the B.S. degree from the Beijing University of Aeronautics and Astronautics in 1985 and the M.S. and Ph.D. degrees from the National University of Defense Technology (NUDT), Changsha, China, in 1988 and 1998, respectively. Since 1988, he has been carrying out teaching and research at NUDT, where he became a Teaching Assistant in 1988, a Lecturer in 1991, an Associate Professor in 1994, and a Professor in 1998. He is currently a Professor and a Ph.D. Supervisor with the College of Mechatronic Engineering and Automation, NUDT. His research interests include design for testability, testability demonstration, fault diagnosis, and fault prognostics.